Available online at www.sciencedirect.com
SCIENCE DIRECT®
ELSEVIER
Earth and Planetary Science Letters 212 (2003) 321–336
EPSL
www.elsevier.com/locate/epsl

Formation history of CI-like phyllosilicate-rich clasts in the Tsukuba meteorite inferred from mineralogy and noble gas signatures[1]

Daisuke Nakashima [a,*], Tomoki Nakamura [b], Takaaki Noguchi [c]

[a] *Department of Earth and Planetary Sciences, Graduate School of Sciences, Kyushu University, Hakozaki, Fukuoka 812-8581, Japan*
[b] *Department of Earth and Planetary Sciences, Faculty of Sciences, Kyushu University, Hakozaki, Fukuoka 812-8581, Japan*
[c] *Department of Materials and Biological Sciences, Ibaraki University, Bunkyo 2-1-1, Mito 310-8512, Japan*

Received 6 December 2002; received in revised form 10 May 2003; accepted 15 May 2003

Abstract

Fine-grained, angular black clasts with longest dimensions up to 800 μm were found, dispersed in a brecciated region in the Tsukuba meteorite. The clasts, much darker than the dark portions of the light–dark structure in the Tsukuba host, are characterized by the presence of plaquette, spherulitic, and framboidal magnetites and pseudo-hexagonal pyrrhotite. Synchrotron radiation X-ray diffraction analyses showed that the major silicate phases in the clasts are saponite and serpentine. Transmission electron microscopy (TEM) revealed that the phyllosilicates have compositions quite similar to those in the Orgueil CI carbonaceous chondrite. Therefore, mineralogically and chemically, the clasts resemble CI chondrites and are quite different from the host H5-6 chondrite Tsukuba. The clasts serve as an indicator of temperatures during regolith lithification of the Tsukuba parent body, because their mineralogy and noble gas compositions are subject to change during weak heating. The 001 basal spacing of saponite in the clast is 13.2 Å, which indicates that saponite retains interlayer water molecules. This observation and the presence of serpentine suggest that the clasts, as a whole, have never been heated above 500°C. Noble gas analyses showed that the clasts contain large amounts of solar and primordial noble gases. The results of stepwise heating analyses indicate that no apparent thermal loss of noble gases from the clasts occurred, consistent with the mineralogical evidence. TEM observation revealed that the periphery of a clast was transformed into amorphous phases, indicating that only the periphery was heated to 700°C. Based on the results of our analyses, the formation history of the clasts can be evaluated as follows. Constituents of the clasts had been exposed to solar wind on the surface of the CI-chondrite-like parent body and formed the clasts. After ejection from the CI-like parent body, the CI-like meteoroid accreted to the Tsukuba parent body after early thermal metamorphism that reached 700–1000°C. The clasts must have been located in the regolith, because they were found among the light–dark structure in the meteorite and contain abundant solar noble gases. Impacts into the regolith have crushed the clasts into smaller pieces and probably induced lithification of the regolith material. During lithification, the peripheries of the clasts were

* Corresponding author. Tel.: +81-92-642-2668; Fax: +81-92-642-2684.
E-mail address: naka@geo.kyushu-u.ac.jp (D. Nakashima).

[1] Supplementary data associated with this article can be found at doi:10.1016/S0012-821x(03)00282-6

0012-821X/03/$ – see front matter
doi:10.1016/S0012-821X(03)00282-6

heated briefly to 700°C, but the temperature of the interior of the clasts has never exceeded 500°C. This is the first evidence constraining temperature during lithification of the ordinary-chondrite parent-body regolith. Finally, the Tsukuba meteoroid, including the CI-like clasts, was ejected from the Tsukuba parent body and fell onto the Earth after a transit time of 8.1 Ma.

Keywords: CI-like clasts; Tsukuba meteorite; mineralogy; noble gases; lithification

1. Introduction

Xenoliths are foreign clasts that occur in various classes of meteorites and their presence indicates that different types of asteroidal material were mixed in the early solar system. Lipschutz et al. [1] noted that the most common xenoliths in meteorites are CM-carbonaceous-chondrite-like materials. On the other hand, CI-chondrite-like xenoliths, which also contain hydrous silicates, occur in several meteorite types, such as Bholghati howardite [2], Kaidun CR2 chondrite [3], Kapoeta howardite [4], Nilpena ureilite [5], Krymka LL3.1 chondrite [6], CB chondrites Queen Alexandra Range 94411, Hammadah al Hamra 237, CH chondrites Patuxent Range 91546, and Allan Hills 85085 [7]. Thus, CI-like xenoliths are not so rare. However, there appears to be limited evidence for the presence of CI-like xenoliths in ordinary chondrites, although ordinary chondrites are the most common meteorites.

We found some fine-grained black clasts (Fig. 1a) in a region with light–dark structure in the Tsukuba meteorite, which is classified as H5-6 [8,9]. We found, through mineralogical and chemical analyses, that these clasts are CI-like xenoliths. In this paper, we focus on the following three questions: Are there any differences between the clasts and CI chondrites? When did the clasts accrete to the Tsukuba parent body – before early thermal metamorphism or after? How intense were impacts and subsequent heating which resulted in the lithification of the surface regolith material of the Tsukuba parent body? Answers to these questions can give additional insights into the nature of accretionary and lithification processes in asteroid regoliths.

2. Analytical procedures

We found three black clasts within a fragment of the Tsukuba meteorite (Fig. 1a). These clasts were named TC1, TC2, and TC3. TC1 and TC3 were crushed into smaller pieces. Some large pieces were named TC1A, TC1B, and TC3A. Remnants of crushed smaller pieces were gathered and named TCmix. Analytical methods are summarized as follows. (1) Scanning electron microscopy (SEM): TC1A and TC2 were embedded in ethylene glycol, polished with microdiamond paste, and observed by scanning electron microscopes (SEM: JEOL JSM-5800LV and Shimadzu SS-550). Backscattered electron (BSE) imaging was used for SEM studies. (2) Electron microprobe analysis: the chemical compositions of TC1A and TC2 were measured with an electron probe microanalyzer (EPMA: JEOL JXA-733 superprobe) equipped with a wavelength-dispersive X-ray spectrometer (WDS). WDS quantitative chemical analyses of TC1A and TC2 were performed at a 15 kV accelerating voltage and 10 nA beam current with a defocused beam 10 μm in diameter. Analyses of the periphery of TC2 were performed using a 10 nA beam current with a focused beam 2 μm in diameter. (3) Synchrotron radiation X-ray diffraction analysis: TC1B and TC3A were mounted on a thin glass fiber, 5 μm in diameter, and exposed to monochromatic X-rays ($\lambda = 2.1611 \pm 0.0005$ Å) at the Institute of Material Structure Science, High Energy Accelerator Organization (Tsukuba, Japan). A clear X-ray powder photograph of a clast can be taken by using a Gandolfi camera with an exposure to synchrotron X-rays of less than 30 min [10]. (4) Transmission electron microscopy (TEM): After X-ray diffraction analysis, TC3A was embedded in epoxy resin and microtomed by a Leitz-Reichert Super Nova ultramicrotome

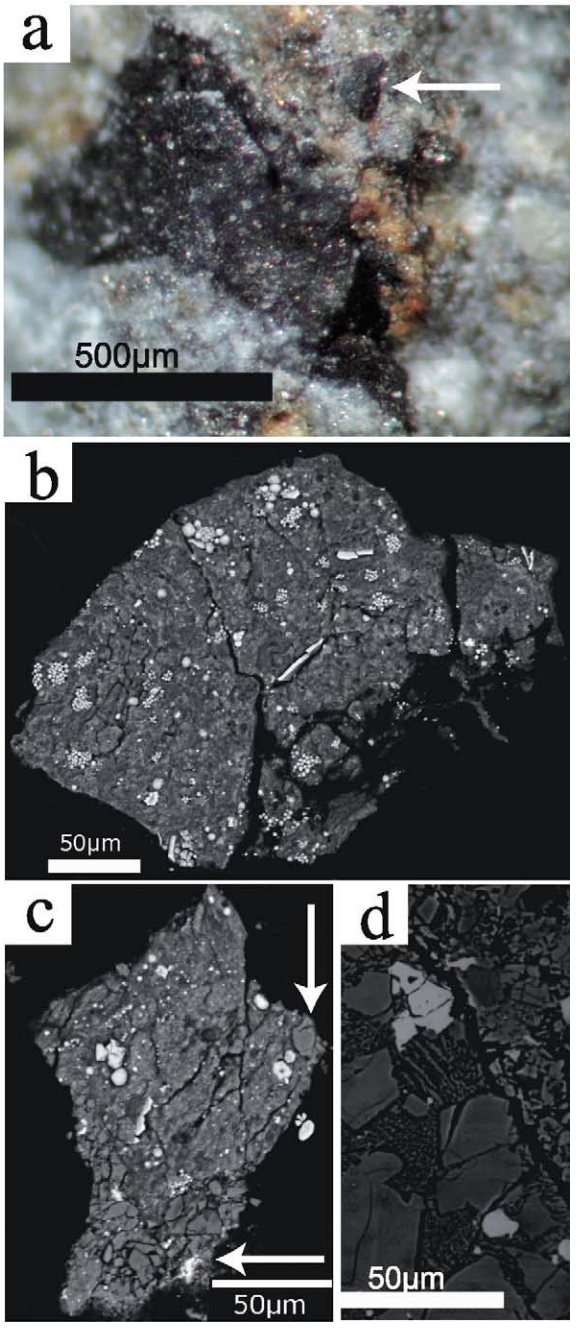

Fig. 1. (a) A stereomicroscope image of the largest clast TC1 (800 μm in diameter) and a small clast (marked by an arrow) in the light–dark structure in the Tsukuba meteorite. (b) A BSE image of TC1A, showing that magnetite framboids and pyrrhotite plates are dispersed in fine-grained materials. (c) A BSE image of TC2 with the host (marked by arrows). (d) A BSE image of the Tsukuba host, showing coarse-grained olivine, pyroxene, and other minerals.

for transmission electron microscopy (JEOL JEM-2000FX II). Quantitative elemental analyses were performed using a Philips DX4 energy-dispersive spectrometer (EDS) system, mounted on the TEM. Detailed TEM procedures are given in [11]. Ultramicrotomy and TEM observation were performed at the Center for Instrumental Analysis, Ibaraki University. For the qualitative analysis of light elements, especially F, we used a JEM-2010F TEM equipped with a JEOL JED-2300T EDS ultrathin window detector. The light-element qualitative analysis was performed at JEOL Ltd., Tokyo, Japan. (5) Noble gas analysis: TCmix (0.7 mg) was heated at 600, 1000, 1200, and 1700°C to extract noble gases. The concentrations and isotopic ratios of He, Ne, Ar, Kr, and Xe were measured with a noble gas mass spectrometer at Kyushu University [12]. In addition, noble gases in Orgueil (14.6 mg), and both a light portion (40.6 mg) and a dark portion (67.7 mg) of Tsukuba were measured for comparison. The light and dark portions were located near TC1. The noble gas components were separated on the basis of isotopic ratios. The following indices are used to denote the noble gas components: P (primordial), C (cosmogenic), S (solar), SEP (solar energetic particles), and SW (solar wind). Solar noble gases consist of SW and SEP. For the isotopic ratios of Ne-SEP, -SW, -A, Xe-Q, -HL, -S, -Air, -SEP, and -SW, we used values from selected references: $(^{20}Ne/^{22}Ne,\ ^{21}Ne/^{22}Ne)_{SEP} = (11.2, 0.0295)$, $(^{20}Ne/^{22}Ne,\ ^{21}Ne/^{22}Ne)_{SW} = (13.8, 0.0328)$ from [13]; $(^{20}Ne/^{22}Ne,\ ^{21}Ne/^{22}Ne)_{A} = (8.2, 0.025)$ from [14]; $(^{130}Xe/^{132}Xe = 0.1629$ and $^{136}Xe/^{132}Xe = 0.3188)_{Q}$ from [15]; $(^{130}Xe/^{132}Xe = 0.1542$ and $^{136}Xe/^{132}Xe = 0.6991)_{HL}$ from [16]; $(^{130}Xe/^{132}Xe = 0.53$ and $^{136}Xe/^{132}Xe = 0)_{S}$ from [17]; and $(^{130}Xe/^{132}Xe = 0.1514$ and $^{136}Xe/^{132}Xe = 0.3294)_{Air}$ from [18]; $(^{130}Xe/^{132}Xe = 0.1513$ and $^{136}Xe/^{132}Xe = 0.3172)_{SEP}$ from [13]; and $(^{130}Xe/^{132}Xe = 0.1656$ and $^{136}Xe/^{132}Xe = 0.2970)_{SW}$ from [13].

3. Mineralogy and chemistry

3.1. General features

TC1A is composed of coarse-grained magnetite

(1–5 μm in diameter) and some sulfides (5–30 μm in diameter) set in a groundmass of fine-grained mineral phases (Fig. 1b). X-ray diffraction analyses (Fig. 2a) and TEM observation showed that the fine-grained phases consist mainly of saponite (typically 10–30 nm in width), serpentine (typically 10–30 nm in width), magnetite (< 100 nm in diameter), and sulfides (typically 200 nm in diameter), with minor amounts of ferrihydrite, chromite, fluorapatite, fluorite, olivine, and low-Ca pyroxene. The grain sizes of minor phases in the clasts are less than 1 μm. TC2 is similar to TC1A (Fig. 1c). The texture of TC1A and TC2 is quite similar to that of Orgueil [19] and is quite different from that of the Tsukuba host (Fig. 1d).

Defocused-beam electron microprobe analyses of the fine-grained mineral phases in TC1A and TC2 show low totals (average 81.9 ± 1.6 wt%), indicating the presence of hydrous minerals. Major element compositions of the mineral phases in TC1A and TC2 show a large variation in Fe/(Si+Al) ratios but a small variation in Mg/(Si+Al) ratios (Fig. 3a). Such compositional variation is similar to that observed in Orgueil [19].

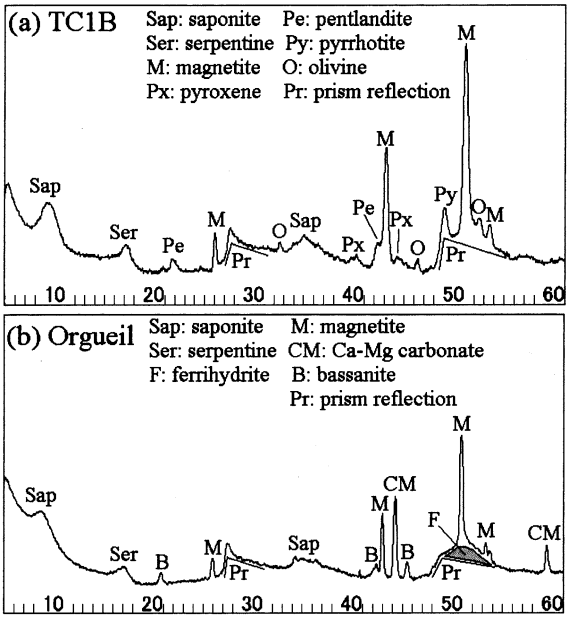

Fig. 2. Synchrotron radiation X-ray diffraction patterns of TC1B (a) and Orgueil (b) in a range of diffraction angles (2θ) from 5 to 60°.

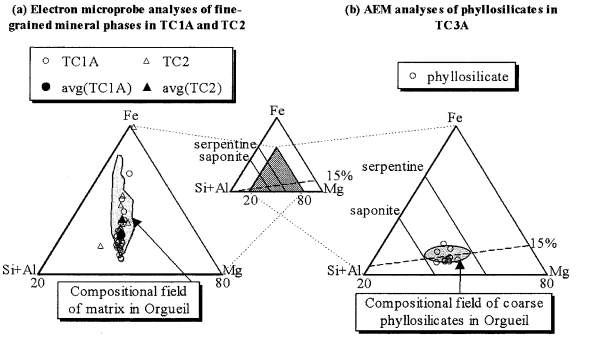

Fig. 3. (a) Electron microprobe analyses of fine-grained mineral phases of TC1A and TC2 in terms of atomic ratios of (Si+Al), Fe, and Mg. The compositional field of matrix in Orgueil [19] is shown for comparison. (b) AEM microanalyses (atom%) of phyllosilicates. Also shown are the ideal Mg–Fe solid solution lines of serpentine ($(Mg,Fe)_6(Si,Al)_4O_{10}(OH)_8$) and saponite ($(Mg,Fe)_3(Si,Al)_4O_{10}(OH)_2$). Analyses of phyllosilicates lie near the broken line defined by Fe/(Mg+Fe) = 15 atom%. The compositional field of coarse phyllosilicates in Orgueil [19] is shown for comparison.

3.2. Opaque minerals

Fig. 4a shows that there are plaquette, spherulitic, and framboidal magnetites in TC1A. The spherulitic magnetite, which is the largest magnetite in Fig. 4a, shows a euhedral, octahedral morphology. Framboidal magnetite morphologies occur in CI, CM, CR, and CV chondrites [20–23]. Plaquettes occur in CI and CR chondrites and the Tagish Lake CI2 chondrite [20,22,24].

A pyrrhotite in TC1A exhibits the euhedral, hexagonal morphology (Fig. 4b). Fig. 4c shows a pyrrhotite plate from TC1A. Pyrrhotites are the most common sulfides in CI chondrites [25]. Electron microprobe analyses show that most of the pyrrhotites contain around 0.6–0.9 atom% Ni, but in some cases they contain rather high concentrations of Ni up to 9 atom%. Such Ni-bearing pyrrhotites also occur in CI-like clasts in Bholghati [2], those in Nilpena (up to 7 atom% Ni; [5]), and CM chondrites [24]. Pentlandite with Ni content of 24.3 atom% occurs in TC1A. Pentlandite is rare in CI chondrites and has been found only in Revelstoke [26] and Alais [25]. Sulfides in TC1A and TC3A show similar compositions (Fig. 5). The clasts contain pure pyrrhotites, Ni-

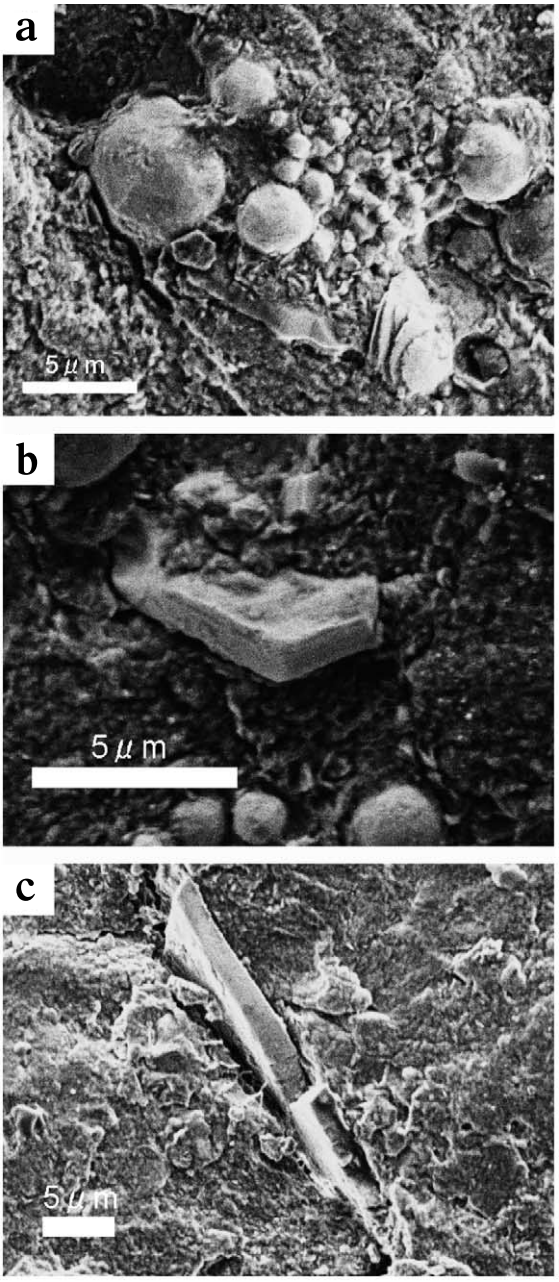

Fig. 4. (a) An enlarged BSE image of plaquette, spherulitic, and framboidal magnetites in TC1A. A plaquette magnetite is on the lower right. A framboidal magnetite is in the center. Four spherulitic magnetites surround the framboidal magnetite. (b) An enlarged BSE image of hexagonal pyrrhotite in TC1A. (c) An enlarged BSE image of a pyrrhotite plate in TC1A.

bearing pyrrhotites, and pure pentlandites (Fig. 5). The mineralogy of the sulfides is similar to that observed in Tagish Lake [24].

The amount of ferrihydrite appears to be small in the clasts, because ferrihydrite cannot be identified in an X-ray diffraction pattern of TC1B (Fig. 2a), and also it is rarely found in TC3A by TEM observation.

We found some accessory phases: chromite ($(Mg, Fe)_2Cr_2O_4$), fluorapatite ($Ca_5(PO_4)_3F$) (Fig. 6a), and fluorite (CaF_2) (Fig. 6b) in TC3A. There are no previous descriptions of fluorapatite and fluorite in other chondrites. The Mg/(Mg+Fe) ratio of the chromite in TC3A is 0.86. The chromite is close to magnesiochromite ($Mg_2Cr_2O_4$) that was found in Orgueil [27]. The Mg/(Mg+Fe) ratios of chromites in ordinary chondrites are about 0.1 [28]; thus it is likely that the chromite in TC3A is indigenous to the clasts and not to the host H chondrite.

3.3. Silicate minerals

The X-ray diffraction pattern of TC1B shows that major silicates are saponite and serpentine (Fig. 2a), which are common in CI chondrites [19,29]. The diffraction patterns of TC1B (Fig. 2a) and TC3A are quite similar to that of Orgueil (Fig. 2b). The relative abundance in TC1B (sap/(sap+ser) = 0.8) is comparable with that of Orgueil (0.7). The relative abundance of saponite and serpentine is defined here as the ratio of the integrated intensity, which is the background-subtracted intensity, of the saponite 001 reflection to that of the serpentine 001 reflection in an X-ray diffraction pattern.

We observed the phyllosilicates in TC3A with TEM. Fig. 7a shows a cluster of phyllosilicates. The phyllosilicate cluster shown in Fig. 7a is quite similar to the coarse phyllosilicates observed in Orgueil [19]. Most saponite and serpentine occur as separate crystals, and their typical size is 10–30 nm thick normal to their 001 planes and less than 200 nm long (Fig. 7b–d). Some of them occur as intergrowths – intimately mixed crystals (Fig. 7c). The characteristic of phyllosilicates in the clasts is that most of the saponite and serpentine occur as

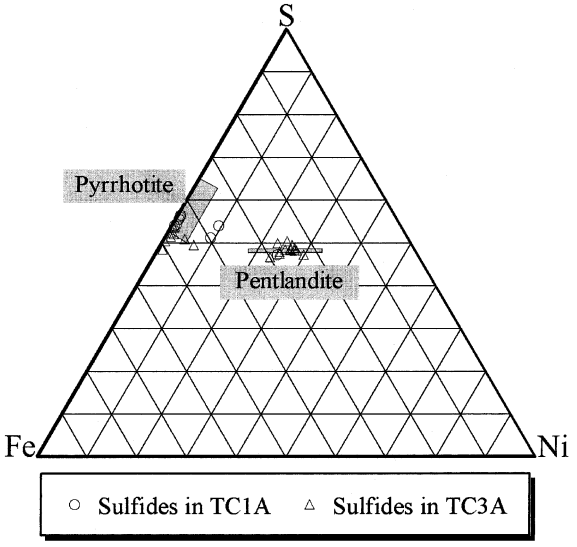

Fig. 5. Compositions of sulfides in TC1A and those in TC3A displayed in a Fe–Ni–S atom% ternary diagram. Sulfides in TC1A were measured with EPMA, and those in TC3A were measured with AEM. Compositional fields of stoichiometric pentlandite and pyrrhotite are shown for comparison.

discrete, separate crystals. Very fine-grained phyllosilicate less than 2–3 nm thick is rare in TC3A.

Compositions of saponite and serpentine could not be determined by analytical electron microscope (AEM) analysis, because individual phyllosilicate grains are much smaller than the diameter of the electron beam (300 nm). Thus, compositions were obtained as averages of the saponite and serpentine crystals under the beam (Fig. 3b). The compositional field of the phyllosilicates in a (Si+Al)–Fe–Mg (atom%) ternary diagram is quite similar to that of the coarse phyllosilicates in Orgueil [19]. Phyllosilicates in TC3A lie on or close to a line with a constant Fe/(Mg+Fe) ratio (=0.15), which suggests that the phyllosilicates are consistently Mg-rich.

The Mg/(Mg+Fe) ratios of olivine (0.815) and low-Ca pyroxene (0.825) found in TC3A by TEM observation are close to those of olivine (0.827) and low-Ca pyroxene (0.843) in the Tsukuba host, respectively the olivine grain exhibited screw dislocations parallel to the *c*-axis, which suggests shock deformation [30]. Therefore, olivine and low-Ca pyroxene seem to be indigenous to the host and injected into the clasts.

3.4. Noble gases

Results of noble gas analyses of TCmix, Orgueil, a light portion of Tsukuba (hereafter Light), and a dark portion of Tsukuba (hereafter Dark) are shown in Tables 1–4[2]. Ne isotopic ratios in TCmix, Light, and Dark are distributed in a triangular area defined by Ne-SW, -SEP, and -cosmogenic components (Fig. 8), showing that Ne in TCmix, Light, and Dark are mixtures of solar Ne and cosmogenic Ne. This is consistent with previous results [9,31]. Ne isotopic ratios in Orgueil are distributed in a triangular area defined by Ne-SEP, -A, and -cosmogenic components, except for Ne released at 1200°C that is plotted below Ne-A (Fig. 8a). The low $^{20}Ne/^{22}Ne$ ratio indicates a contribution from Ne-E ($^{20}Ne/^{22}Ne$, $^{21}Ne/^{22}Ne = 0$, 0) [32]. This is consistent with the results given in [33]. In TCmix, the primordial components (Ne-A and -E) cannot be identified, because these components are masked by a large amount of solar Ne. The presence of solar gases in TCmix suggests that the clasts were exposed to SW on the surface of a parental object, because the penetration depth of SW particles is only several hundred Å [34]. The details of SW exposure to the clasts are discussed in Section 4.

Ne was separated into solar, cosmogenic, and primordial components on the basis of Ne isotopic ratios, the ^{132}Xe concentration, and the primordial $^{20}Ne/^{132}Xe$ ratio, as shown in the Appendix. The concentrations of solar ^{20}Ne ($^{20}Ne_S$), cosmogenic ^{20}Ne ($^{20}Ne_C$), and primordial ^{20}Ne ($^{20}Ne_P$) in TCmix, Orgueil, Light, and Dark are shown in Fig. 9a. This figure shows that Ne in TCmix is dominated by solar gases.

The ^{132}Xe concentration in TCmix is comparable with that in Orgueil, whereas those in Light and Dark are one order of magnitude smaller than that in TCmix (Fig. 9b). Fig. 10 shows a Xe three-isotope diagram. Xe isotopic ratios released from TCmix at 1000 and 1200°C are distributed on a Q–HL line. In Orgueil, the isotopic ratio of Xe released at 1000°C is also distributed on the Q–HL line, whereas Xe isotopic ratios re-

[2] See the online version of this article.

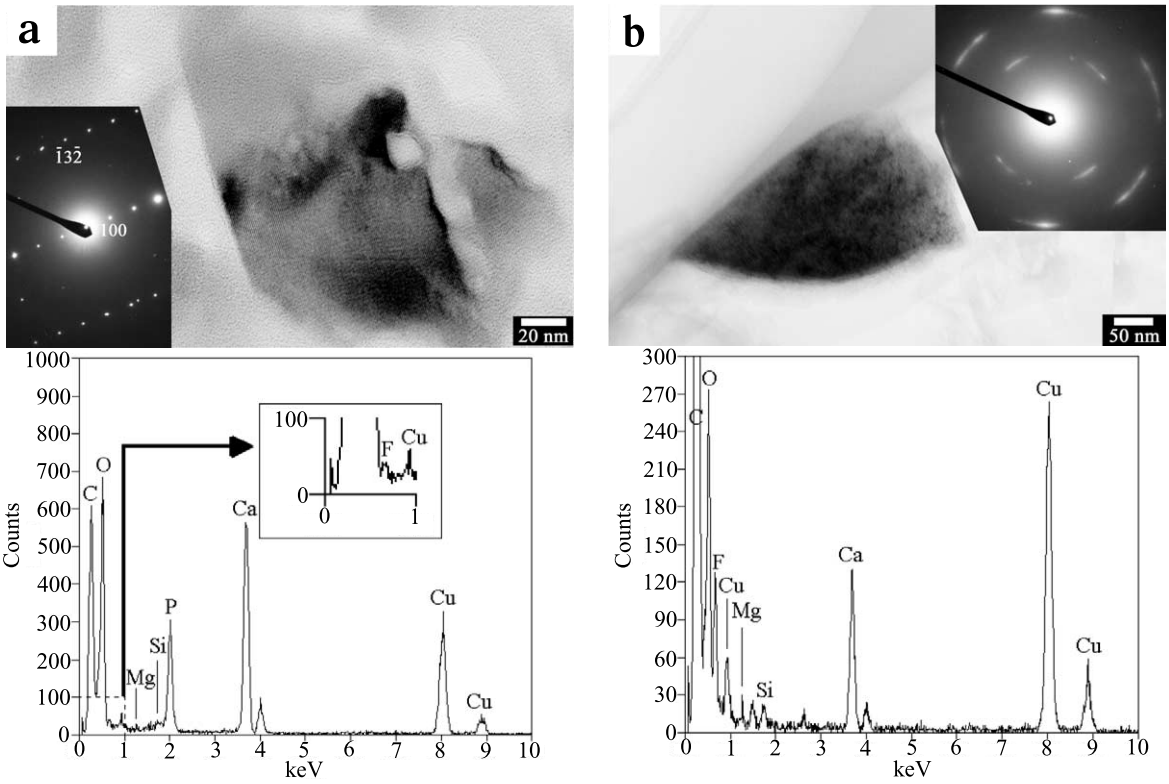

Fig. 6. (a) A TEM micrograph of fluorapatite ($Ca_5(PO_4)_3F$). Insets are a selected-area electron diffraction (SAED) pattern and a TEM-EDS spectrum. The TEM-EDS spectrum shows strong Ca and P lines and a weak F line. (b) A TEM micrograph of fluorite (CaF_2). Insets are a SAED pattern and a TEM-EDS spectrum. The TEM-EDS spectrum shows strong Ca and F lines as well as weak Si and Mg lines from the surrounding phyllosilicates. TEM-EDS spectra in panels a and b show strong CKα and OKα lines, because fluorapatite and fluorite are embedded in epoxy resin, mounted on plastic film, and deposited by carbon vapor. Cu lines are from Cu grids.

leased at 600, 1200, and 1700°C are distributed around Q. Therefore, Xe in both TCmix and Orgueil consists predominantly of Xe-Q with a minor amount of Xe-HL. The ^{132}Xe-HL contributes approximately 2% and 1% to the total ^{132}Xe in TCmix and Orgueil, respectively. The ^{132}Xe-HL contribution in TCmix and Orgueil is comparable with that in the Yamato-791198 CM chondrite (2%; [35]) and that in Tagish Lake (2%; [10]). Thus, the Xe-HL/Xe-Q ratio in the clasts is similar to that in hydrous carbonaceous chondrites. This may imply that Xe-HL/Xe-Q ratios in dust in the regions where hydrous carbonaceous chondrites formed were roughly constant. In summary, the clasts are quite similar to Orgueil with respect to their heavy noble gas signatures.

4. Discussion

4.1. Differences between the clasts and the Tsukuba host

We summarize here the main differences between the clasts and the Tsukuba host: (1) only the former contains hydrous silicates, (2) only the latter contains chondrules, and (3) the former contains magnetite, but the latter contains Fe–Ni metal. Therefore, mineralogically and petrologically the clasts differ significantly from the Tsukuba host.

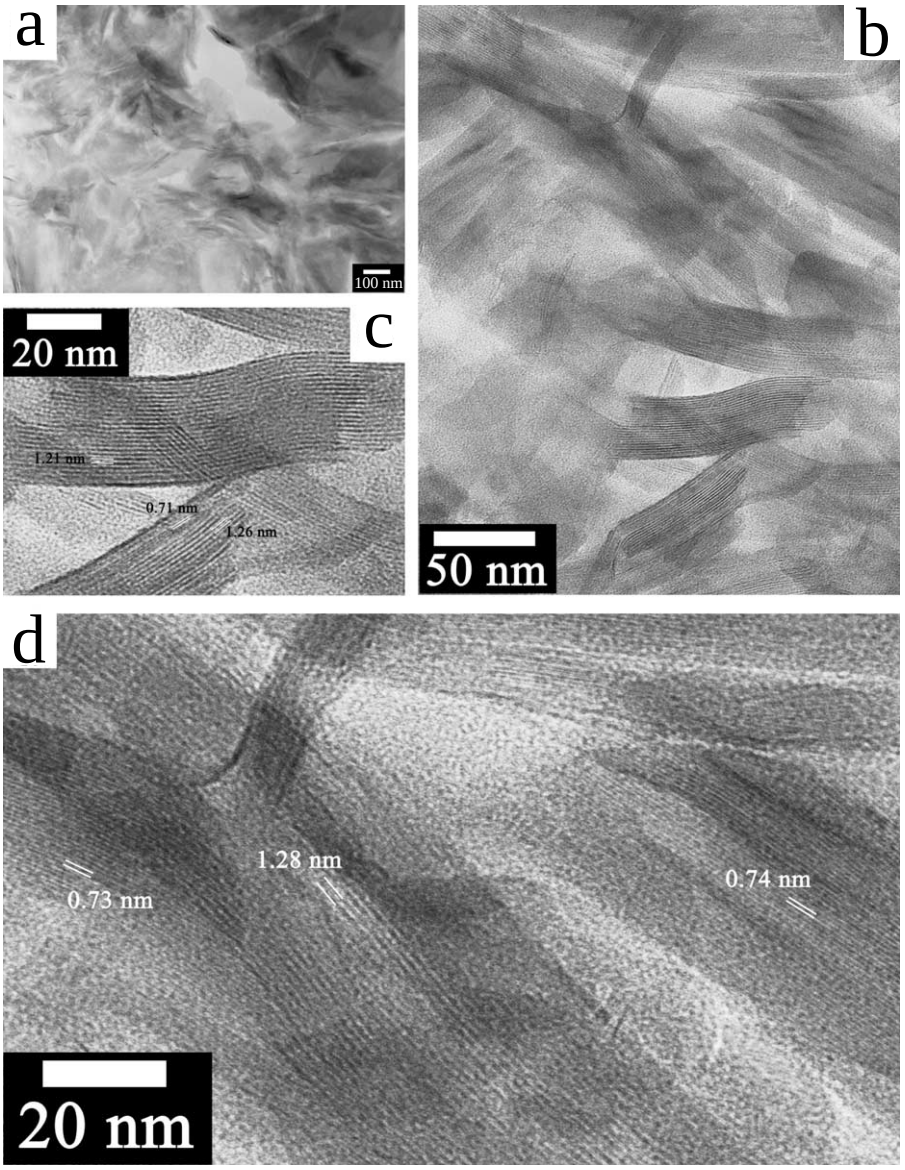

Fig. 7. (a) A TEM photomicrograph showing an area composed of phyllosilicates. (b) A high-resolution TEM image showing a phyllosilicate cluster. (c) An enlarged image of the bottom in panel b showing saponite crystals and interstratified saponite and serpentine crystals. (d) An enlarged image of the top in panel b showing crystals of saponite and serpentine.

4.2. *Similarities and differences between the clasts and CI chondrites*

In this subsection, similarities and differences between the clasts and the CI chondrites Orgueil and Ivuna are summarized. The reason why Orgueil and Ivuna are used for comparison is that they have been widely and intensively studied. Similarities between the clasts and these meteorites are summarized as follows. (1) Framboidal and plaquette magnetites are present. (2) Major silicate minerals are saponite and serpentine.

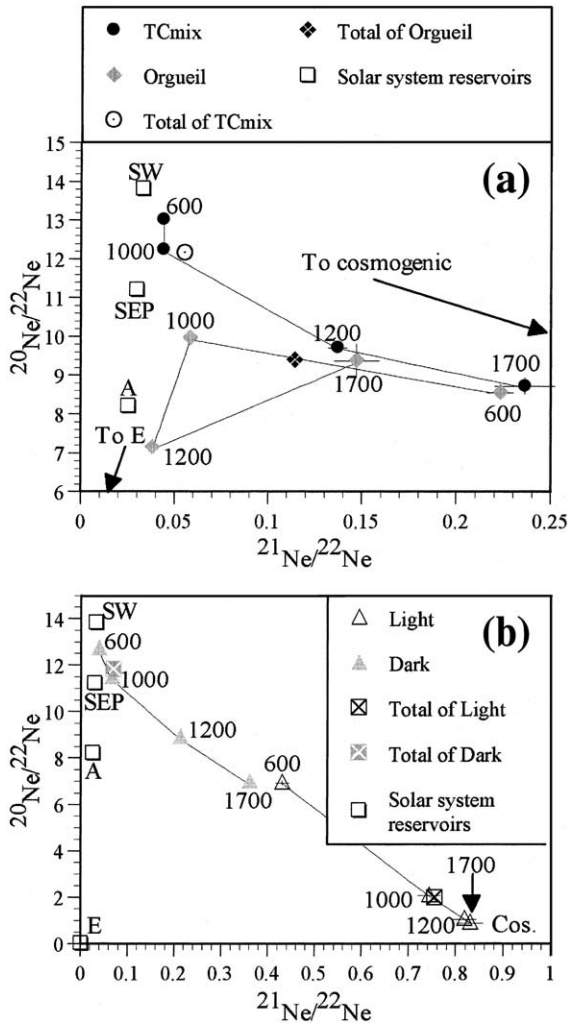

Fig. 8. Ne three-isotope-diagrams showing the results of stepwise heating analyses of (a) TCmix and Orgueil and (b) Light and Dark. The numerals near the data points refer to the temperature in °C. Abbreviation in panel b: Cos, cosmogenic.

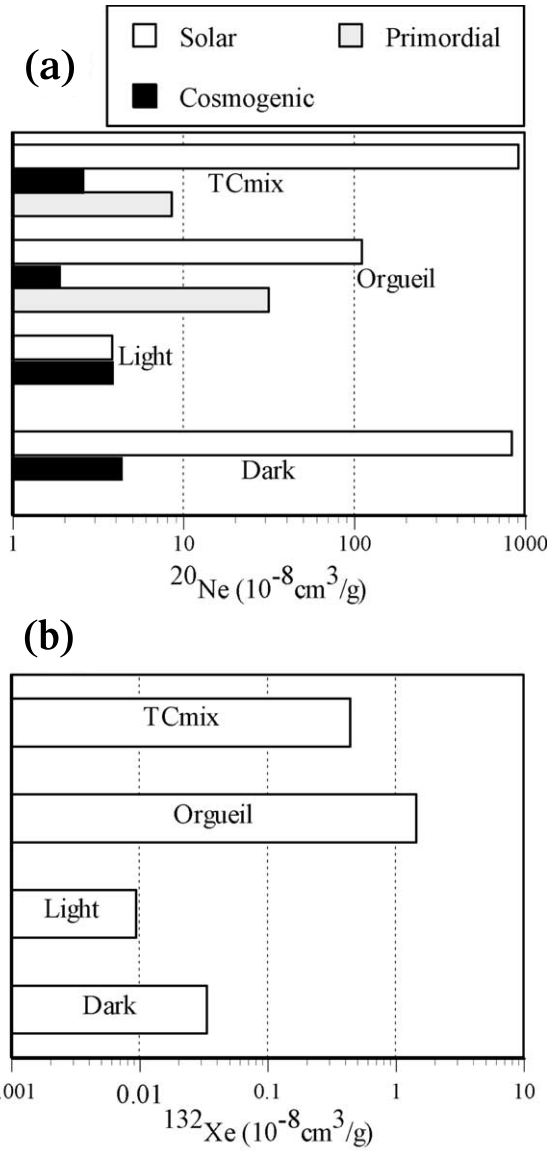

Fig. 9. (a) The $^{20}Ne_S$, $^{20}Ne_C$, and $^{20}Ne_P$ concentrations of TCmix, Orgueil, Light, and Dark. (b) The ^{132}Xe concentrations in TCmix, Orgueil, Light, and Dark.

The relative abundance of saponite and serpentine in TC1B (sap/(sap+ser) = 0.8) is comparable with that in Orgueil (0.7). (3) Phyllosilicates are richer in Mg than Fe; the Fe/(Fe+Mg) ratio of phyllosilicates in TC3A is close to those in Orgueil (0.15; [19]) and Ivuna (~0.20; [36]). (4) Heavy noble gases are dominated by a primordial component. The Xe-HL/Xe-Q ratio in TCmix is comparable with that in Orgueil. (5) The clasts and CI chondrites lack chondrules, and anhydrous silicate minerals are extremely rare in both of them.

On the other hand, differences between the clasts and CI chondrites Orgueil and Ivuna are summarized as follows. (1) The amount of ferrihydrite appears to be small in the clasts. Instead of ferrihydrite, many fine-grained magnetite and sulfides were found in the clasts by TEM obser-

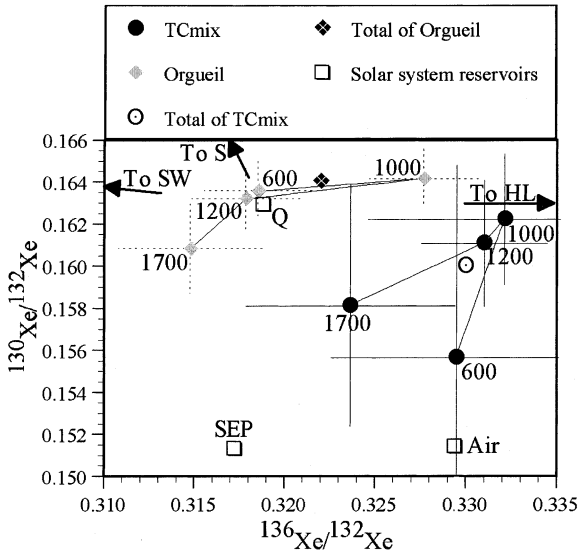

Fig. 10. A Xe three-isotope diagram showing the results of stepwise heating analyses of TCmix and Orgueil. The numerals near the data points refer to the temperature in °C. In TCmix, the isotopic ratios of Xe in 600 and 1700°C fractions are distributed on the Q–Air line, because of the large atmospheric Xe contribution. Xe data of Light and Dark are not plotted, because the errors of Xe isotopic ratios from these samples are too large.

vation. There are large variations in Fe contents in the fine-grained mineral phases in TC1A and TC2 (Fig. 3a). Tomeoka and Buseck [19] noted that the Fe variations in Orgueil are attributed to the presence of ferrihydrite. In the case of the clasts, however, the variations are attributable to the abundances of fine-grained magnetite and sulfides. In this respect, the clasts are different from Orgueil. The clasts are similar to Ivuna in that the amount of ferrihydrite appears to be small. However, Fe variations are not observed in Ivuna [36]. (2) Most of the saponite and serpentine occur as discrete, separate crystals. On the other hand, most of the saponite and serpentine in Orgueil and Ivuna occur as intergrown crystals [19,36]. These data indicate that the clasts are quite similar to CI chondrites Orgueil and Ivuna in many important respects, but they differ from CI chondrites in some minor respects. Therefore, in the following discussion, we refer to the clasts as 'CI-like clasts'.

4.3. Imprints of heating found in the CI-like clasts

The CI-like clasts were found among the light–dark structure in the Tsukuba meteorite. The light–dark structure was formed by impact processes into the surface regolith of the meteorite parent body [37–44]. Hence, the clasts must have been located in the regolith and affected by impacts and subsequent heating that resulted in lithification of the regolith. In this subsection, we discuss the degrees of shock and heating experienced by the clasts.

First, we show three lines of evidence that constrain the temperature of heating. (1) The survival of serpentine in the clasts: Fig. 11a compares X-ray diffraction data for the 001 reflection of serpentine in TC1B with similar data for an unheated Orgueil sample and Orgueil samples heated to 200–800°C [45]. When Orgueil was heated to 600°C, the 001 reflection of serpentine disappeared. In TC1B, the 001 reflection of serpentine is clearly observed. This shows that the clasts have never experienced heating to 600°C. (2) The preservation of interlayer water molecules in saponite: Fig. 11b shows the 001 basal spacing of saponite from the same series of samples as in Fig. 11a [45]. The 001 basal spacing of saponite in Orgueil samples is almost constant for samples heated to 500°C. Shrinkage of the 001 spacing occurs in Orgueil heated to 600°C due to the loss of interlayer water molecules. The 001 basal spacing of saponite in TC1B is similar to that in unheated or weakly heated Orgueil (up to 500°C). This result suggests that the clasts have never experienced heating above 500°C. (3) No apparent thermal loss of solar noble gases: Fig. 12 shows the concentrations and isotopic ratios of He and Ne released from TCmix during stepwise heating analyses. In the 600°C fraction, large amounts of solar He and Ne were released. This indicates that the clasts have never experienced heating above 600°C. From the evidence in (1)–(3), we concluded that the clasts have never experienced heating above 500°C.

Next, we discuss the imprint of heating at the peripheries of the clasts. To identify the presence of structural water in phyllosilicates at the periphery, the major element concentrations of phyllo-

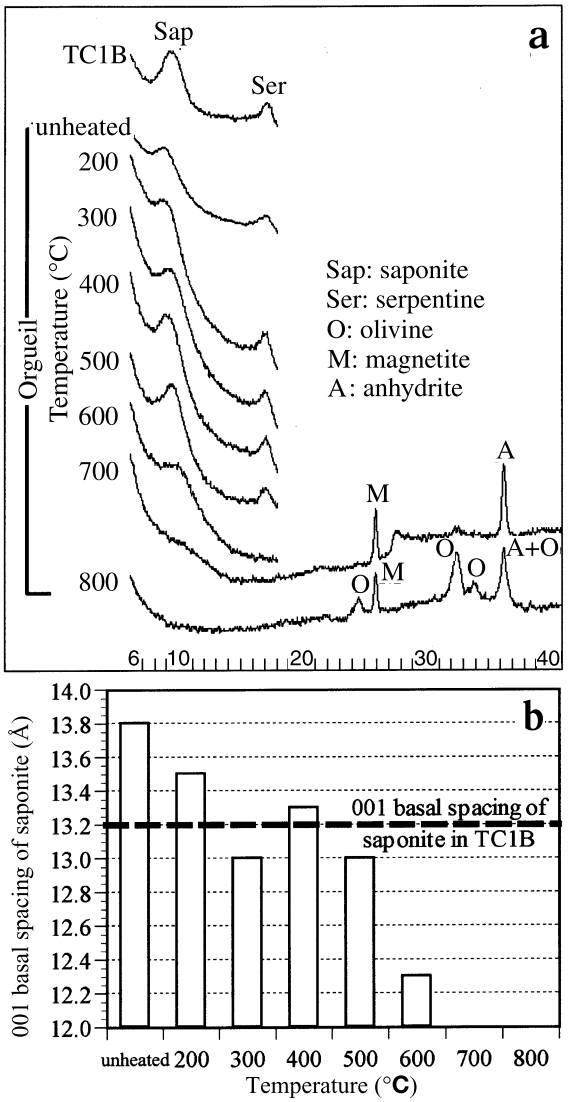

Fig. 11. (a) Synchrotron radiation X-ray diffraction patterns of TC1B, unheated Orgueil sample, and Orgueil samples heated to 200–800°C in vacuum, in a range of diffraction angles from 6 to 18° (700 and 800°C: 6–40°). The heating duration of Orgueil is approximately 1 min. (b) The 001 basal spacing of saponite from the same series of Orgueil as in panel a. The broken line represents the 001 basal spacing of saponite in TC1B.

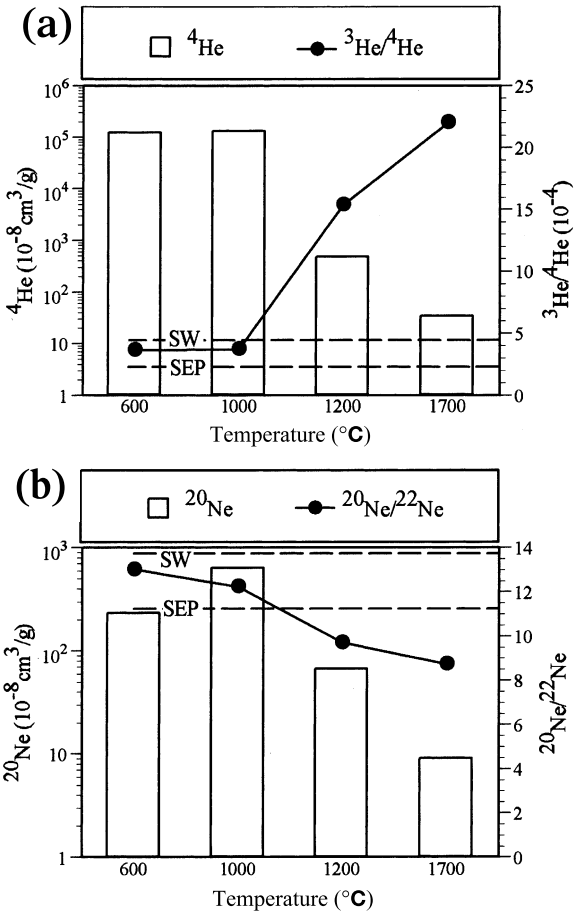

Fig. 12. (a) The ^{4}He concentrations and ^{3}He/^{4}He ratios released from TCmix during stepwise heating analyses. (b) The ^{20}Ne concentrations and ^{20}Ne/^{22}Ne ratios released from TCmix during stepwise heating analyses. The broken lines in panels a and b represent isotopic ratios of SW and SEP [13].

silicates, which are located near the boundary between the clast TC2 and the host, were measured with a 2 μm-focused beam of an electron microprobe (Fig. 1c). Totals of major element concentrations of dehydrated phyllosilicates in the Yamato-86789 CM chondrite are close to 100 wt% [46]. Therefore, if the phyllosilicates at the peripheries of the clasts are dehydrated, the totals must be close to 100 wt%. However, the analytical total of material at the periphery of TC2 is 84.5 ± 3.3 wt% on average. The average total of material in the interior of TC1A and TC2 is 81.9 ± 1.6 wt% (see Section 3). There is no difference within 1σ variations between the total for the periphery of TC2 and that for the interior of TC1A and TC2. Therefore, it seems that the peripheries of the

clasts are not dehydrated. To inspect the microtexture of the periphery, we observed a clast with TEM. At the periphery, minerals from the clast and the host are intimately mixed (Fig. 13a), exhibiting a zigzag contact. The layer structures of phyllosilicates, as observed in the central parts of the clasts (Fig. 7), almost disappeared (Fig. 13b), indicating that the phyllosilicates have been transformed into amorphous substance. This amorphous substance is typical of material formed during thermal transformation from phyllosilicates into anhydrous silicates. As shown in Fig. 11a, the 001 reflections of both saponite and serpentine cannot be identified in Orgueil heated to 700 and 800°C, and reflections of olivine are absent at 700°C, but appear at 800°C. This indicates that phyllosilicates in Orgueil heated to 700°C were transformed into an amorphous substance, and the amorphous substance recrystallized into olivine at 800°C. Therefore, the amorphous state of phyllosilicates at the peripheries of the clasts indicates that these were heated to 700°C. In summary, although the interior of the clasts has never experienced heating above 500°C, the peripheries of the clasts were heated to 700°C. Such heterogeneous temperature distributions can be achieved by brief heating induced by impacts. When an impact occurred on the meteorite parent body, it must have compressed the regolith. Mineral particles in the regolith crushed each other, and friction occurred along boundaries between the particles. Similar frictional heating must have occurred between the clasts and the host minerals in the same manner observed in a chondrite regolith breccia [47]. Finally, the regolith was lithified.

The shock intensity experienced by the clasts can be estimated. As mentioned above, the peripheries of the clasts are not dehydrated. Therefore, the clasts, as a whole, were not dehydrated. It is reported that impact-induced dehydration of phyllosilicates in the Murchison CM chondrite begins at a shock pressure of about 10 GPa [48]. Therefore, the upper limit of shock pressure experienced by the clasts is 10 GPa.

Finally, we infer the timing of incorporation of the clasts into the Tsukuba parent body. The Tsukuba meteorite is classified as H5-6 [8,9]. The temperature of early thermal metamorphism occurring in the H5-6 chondrite parent body is supposed to be 700–1000°C [49]. On the other hand, our results showed that the clasts have never experienced heating at a temperature higher than 500°C. Therefore, it can be concluded that the clasts accreted after the peak of thermal metamorphism.

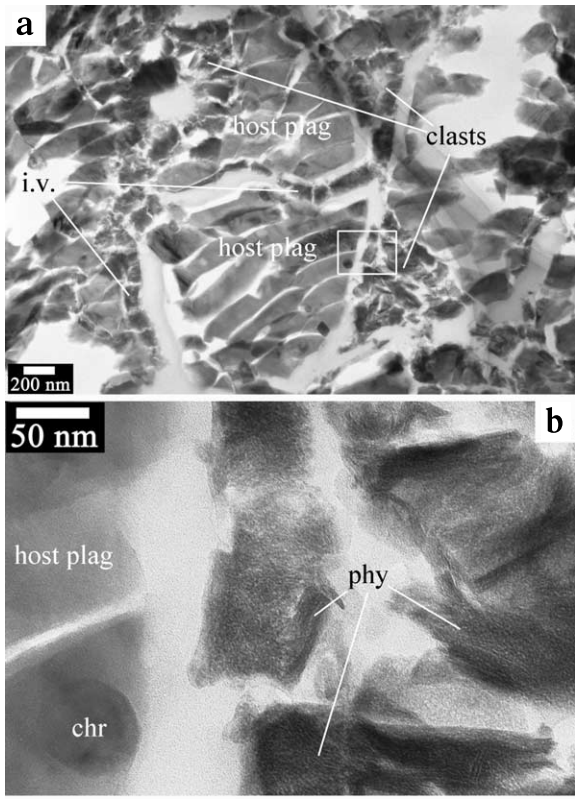

Fig. 13. (a) A low-magnification TEM photomicrograph of the periphery between a clast and the host. There are some sinuous veins made of small clasts. These veins were probably injected during lithification. (b) An enlarged image of panel a, boxed area, showing phyllosilicates whose layer structures have almost disappeared. Abbreviations: host plag, plagioclase from the host; i.v., injected vein of the CI-like clast material; chr, chromite; phy, phyllosilicate.

4.4. *Where did the clasts acquire solar noble gases?*

In this subsection, we discuss where the clasts acquired solar noble gases. First, four lines of evidence necessary for the discussion are shown. (A) When the shock-induced lithification occurred

in the regolith on the Tsukuba parent body, the peripheries of the clasts were heated to 700°C and probably lost the solar gases. (B) The results of stepwise heating analyses showed that the clasts released large amounts of solar gases at 600°C. (C) The penetration depth of SW is only several hundred Å [34]. (D) The size of the clasts is several hundred μm. The evidence from (A) and (B) indicates that the interior of the clasts retained large amounts of solar gases. The evidence of (C) and (D) indicates that SW cannot reach the interior of the clasts after the clasts were consolidated. These two facts, therefore, suggest that the clasts were formed by consolidation of the materials already enriched in solar gases. Where, then, did the solar-gas-rich materials acquire solar gases? Our results showed that the mineralogy of the clasts is identical to that of CI chondrites. Therefore, the constituents of the clasts must have been exposed to SW and acquired solar gases on the surface of the CI-like parent body.

4.5. Formation history of CI-like clasts

Based on the results of a series of analyses, we have evaluated the formation history of the CI-like clasts in the Tsukuba meteorite. Constituents of the clasts had been exposed to SW on the surface of the CI-like parent body and formed the clasts. The exposure must have occurred after aqueous alteration, because the low-energy SW component, which was lost from mineral surfaces during the aqueous alteration [50], is still retained in the interior of the clasts. After ejection from the CI-like parent body, the CI-like meteoroid accreted to the Tsukuba parent body after the peak of thermal metamorphism. The clasts were located in the regolith and may have been exposed to SW, because they were found in the light–dark structure of the Tsukuba meteorite. Impacts into the regolith with shock pressures less than 10 GPa have crushed the clasts into smaller pieces and induced lithification of regolith material. During lithification, the peripheries of the clasts were heated briefly to 700°C. Finally, the Tsukuba meteoroid, including the clasts, was ejected from the Tsukuba parent body and fell onto the Earth after a transit time of 8.1 Ma [9].

5. Conclusions

(1) Mineralogically and compositionally, the fine-grained black clasts in the Tsukuba H5-6 chondrite resemble CI chondrites. The clasts, however, differ from Orgueil and Ivuna in minor respects such as the texture of saponite and serpentine.

(2) The interior of the clasts has never been heated to a temperature higher than 500°C. This suggests that the CI-like meteoroid accreted to the Tsukuba parent body after the peak of thermal metamorphism.

(3) Only the peripheries of the clasts were heated to 700°C. This indicates that a short period of heating, induced by impacts, resulted in the lithification of the regolith material of the Tsukuba parent body.

Acknowledgements

We thank three referees (Drs. G. R. Huss, J. A. Whitby, and A. J. Brearley) for constructive comments, Dr. M. Watanabe for technical support in SEM observation at the Center of Advanced Instrumental Analysis in Kyushu University, Mr. K. Shimada for technical support in the electron microprobe analysis, Drs. M. Tanaka, W. Nozaki, and T. Mori for technical support during X-ray diffraction analysis at the Institute of Material Structure Science, the High Energy Accelerator Organization (Tsukuba, Japan), and JEOL Ltd., Tokyo, Japan for their permission to use JEM-2010F. Mr. N. Endo is appreciated for his technical assistance during EDS analysis using JEM-2010F. We also thank Dr. M. E. Zolensky for constructive comments.***[BOYLE]***

Appendix

The calculation sequences, in order to obtain the $^{20}Ne_S$, $^{20}Ne_C$, and $^{20}Ne_P$ concentrations of TCmix, Orgueil, Light, and Dark, respectively, are shown below.

TCmix: Before the calculation, the following assumptions were made: (a) the $^{20}Ne_P$ concentra-

tion is proportional to that of ^{132}Xe with the ratio of $(^{20}Ne/^{132}Xe)_P = 19.4$, given by [50]; (b) Xe in TCmix is completely primordial noble gas; and (c) the isotopic ratio of Ne-cosmogenic ($^{20}Ne/^{22}Ne$, $^{21}Ne/^{22}Ne)_C$ is (0.8, 0.9) from average shielding for chondrites (e.g. [51]). There are two reasons for this assumption (c). The first reason is that the Ne data of TCmix are plotted near Ne-SW and -SEP rather than Ne-cosmogenic (Fig. 8a). The second reason is that the $^{21}Ne/^{22}Ne$ ratio is a function of the meteorite size and shielding depth. We do not know these parameters, because the Tsukuba meteorite fell as a meteorite shower [52]. Therefore, we cannot calculate the isotopic ratio of Ne-cosmogenic in TCmix.

Using the above assumptions, we calculated the ^{20}Ne concentration of each component in the following sequence. (1) The $^{20}Ne_P$ concentration was obtained using the ^{132}Xe concentration and the $(^{20}Ne/^{132}Xe)_P$ ratio (19.4). (2) The primordial Ne, having Ne-A isotopic ratio and concentration determined in step (1), was subtracted from the measured Ne isotopic ratio (point M_1 in Fig. 14) and concentration; then we have Ne (point N_1 in Fig. 14) consisting of solar and cosmogenic Ne (Fig. 14). (3) ($^{20}Ne/^{22}Ne$, $^{21}Ne/^{22}Ne)_S$ (point S_1 in Fig. 14) was determined by taking the intersection of the SW–SEP line and an extension line of Cos. (Ne-cosmogenic) (Fig. 14). We used the following equations to obtain the $^{20}Ne_S$ and $^{20}Ne_C$ concentrations:

$$^{20}Ne_S = {}^{22}Ne_N \frac{(^{21}Ne/^{22}Ne)_N - (^{21}Ne/^{22}Ne)_C}{(^{21}Ne/^{22}Ne)_S - (^{21}Ne/^{22}Ne)_C} \times (^{20}Ne/^{22}Ne)_S \quad (1)$$

$$^{20}Ne_C = {}^{22}Ne_N \frac{(^{21}Ne/^{22}Ne)_S - (^{21}Ne/^{22}Ne)_N}{(^{21}Ne/^{22}Ne)_S - (^{21}Ne/^{22}Ne)_C} \times (^{20}Ne/^{22}Ne)_C \quad (2)$$

where $^{22}Ne_N$ is the ^{22}Ne concentration obtained by correction for $^{22}Ne_P$ from the ^{22}Ne concentration, and ($^{20}Ne/^{22}Ne$, $^{21}Ne/^{22}Ne)_N$ is the isotopic ratio at point N_1 in Fig. 14.

Orgueil: Before the calculation, we made assumption (c), which was used above. The Ne isotopic ratio of Orgueil (point M_2 in Fig. 14) is plotted in the triangular area of SEP, A, and Cos (Fig. 8a). (1) The $^{20}Ne_P$ concentration was obtained by using the following equation:

$$^{20}Ne_P = {}^{22}Ne \frac{(^{21}Ne/^{22}Ne) - (^{21}Ne/^{22}Ne)_N}{(^{21}Ne/^{22}Ne)_A - (^{21}Ne/^{22}Ne)_N} \times (^{20}Ne/^{22}Ne)_A \quad (3)$$

where $(^{21}Ne/^{22}Ne)_N$ is the x-coordinate of point N_2 in Fig. 14 determined by taking the intersection of the SEP–cosmogenic line and an extension line of A, and $(^{21}Ne/^{22}Ne)_A$ is the $(^{21}Ne/^{22}Ne)$ ratio of Ne-A. (2) The $^{20}Ne_S$ and $^{20}Ne_C$ concentrations were obtained using Eqs. 1 and 2, respectively. In Eqs. 1 and 2, the isotopic ratio of SEP is adopted for ($^{20}Ne/^{22}Ne$, $^{21}Ne/^{22}Ne)_S$.

Light and Dark: Ne in Light and Dark was a mixture of solar and cosmogenic components (Fig. 8b). To obtain the $^{20}Ne_S$ and $^{20}Ne_C$ concentrations, we used the two Eqs. 1 and 2. However, $(^{21}Ne/^{22}Ne)_N$ is the x-coordinate of the measured point (M_3 in Fig. 14) and the $^{22}Ne_N$ concentration corresponds to the measured ^{22}Ne concentration, because Ne in Light and Dark does not contain a primordial component. $(^{21}Ne/^{22}Ne)_C$ is regarded

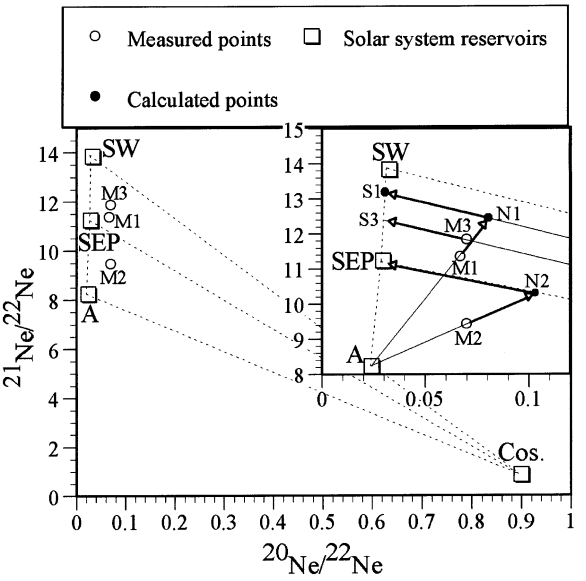

Fig. 14. A Ne three-isotope diagram used for the calculation of Ne concentrations of components solar Ne, cosmogenic Ne, and primordial Ne. Dotted lines connect the solar system reservoirs and Ne-cosmogenic (Cos.), respectively.

as the x-coordinate of the data point of Ne released at 1700°C from Light. $(^{21}Ne/^{22}Ne)_S$ is the x-coordinate of point S_3 in Fig. 14.

References

[1] M.E. Lipschutz, M.J. Gaffey, P. Pellas, Meteoritic parent bodies: Nature, number, size and relation to present-day asteroids, in: R.P. Binzel, T. Gehrels, M.S. Matthews (Eds.), Asteroids II, University of Arizona Press, Tucson, AZ, 1989, pp. 740–777.

[2] A.M. Reid, P.C. Buchanan, M.E. Zolensky, R.A. Barrett, The Bholghati howardite: Petrography and mineral chemistry, Geochim. Cosmochim. Acta 54 (1990) 2161–2166.

[3] M.E. Zolensky, R.A. Barrett, A.V. Ivanov, Mineralogy and matrix composition of CI clasts in the chondritic breccia Kaidun, Lunar Planet. Sci. Conf. XXII, 1991, pp. 1565–1566.

[4] A.J. Brearley, Carbonaceous chondrite clasts in the Kapoeta howardite, Lunar Planet. Sci. Conf. XXIV, 1991, pp. 183–184.

[5] A.J. Brearley, M. Prinz, CI chondrite-like clasts in the Nilpena polymict ureilite: Implications for aqueous alteration processes in CI chondrites, Geochim. Cosmochim. Acta 56 (1992) 1373–1386.

[6] A.L. Girich, V.P. Semenenko, Magnetite-bearing fragments in the Krymka chondrite, Meteorit. Planet. Sci. Suppl. 36 (2001) A66.

[7] A. Greshake, A.N. Krot, A. Meibom, M.K. Weisberg, M.E. Zolensky, K. Keil, Heavily-hydrated lithic clasts in CH chondrites and the related, metal-rich chondrites Queen Alexandra Range 94411 and Hammadah al Hamra 237, Meteorit. Planet. Sci. 37 (2002) 281–293.

[8] J.N. Grossman, The Meteoritical Bulletin, No. 80, 1996 July, Meteorit. Planet. Sci. 31 (1996) A175–A180.

[9] D. Nakashima, T. Nakamura, M. Sekiya, N. Takaoka, Cosmic-ray exposure age and heliocentric distance of the parent body of H chondrites Yamato-75029 and Tsukuba, Antarct. Meteor. Res. 15 (2002) 97–113.

[10] T. Nakamura, T. Noguchi, M.E. Zolensky, M. Tanaka, Mineralogy and noble-gas signatures of the carbonate-rich lithology of the Tagish Lake carbonaceous chondrite: evidence for an accretionary breccia, Earth Planet. Sci. Lett. 207 (2003) 83–101.

[11] T. Noguchi, T. Nakamura, W. Nozaki, Mineralogy of phyllosilicate-rich micrometeorites and comparison with Tagish Lake and Sayama meteorites, Earth Planet. Sci. Lett. 202 (2002) 229–246.

[12] T. Nakamura, N. Takaoka, Solar-wind derived light noble gases in micrometeorites collected at the Dome Fuji Station: Characterization by stepped pyrolysis, Antarct. Meteor. Res. 13 (2000) 311–321.

[13] J.-P. Benkert, H. Baur, P. Signer, R. Wieler, He, Ne and Ar from the solar wind and solar energetic particles in lunar ilmenites and pyroxenes, J. Geophys. Res. 98 (1993) 13147–13162.

[14] R.O. Pepin, Trapped neon in meteorites, Earth Planet. Sci. Lett. 2 (1967) 13–18.

[15] R. Wieler, E. Anders, H. Baur, R.S. Lewis, P. Signer, Noble gases in phase 'Q': Closed-system etching of an Allende residue, Geochim. Cosmochim. Acta 55 (1991) 1709–1722.

[16] G.R. Huss, R.S. Lewis, Noble gases in presolar diamonds I: Three distinct components and their implications for diamond origins, Meteoritics 29 (1994) 791–810.

[17] U. Ott, F. Begemann, J. Yang, S. Epstein, S-process krypton of variable isotopic composition in the Murchison meteorite, Nature 332 (1988) 700–702.

[18] J.R. Basford, J.C. Dragon, R.O. Pepin, M.R. Coscio Jr., V.R. Murthy, Krypton and xenon in lunar fines, Proc. Lunar Sci. Conf. IV, 1973, pp. 1915–1955.

[19] K. Tomeoka, P.R. Buseck, Matrix mineralogy of the Orgueil CI carbonaceous chondrite, Geochim. Cosmochim. Acta 52 (1988) 1627–1640.

[20] J.F. Kerridge, A.L. MacKay, W.V. Boynton, Magnetite in CI carbonaceous meteorites: Origin by aqueous activity on a planetesimal surface, Science 205 (1979) 395–397.

[21] A.M. Davis, E. Olsen, Bells-A carbonaceous chondrite related to C1 and C2 chondrites, Lunar Planet. Sci. Conf. XV, 1984, pp. 190–191.

[22] M.K. Weisberg, M. Prinz, R.N. Clayton, T.K. Mayeda, The CR (Renazzo-type) carbonaceous chondrite group and its implications, Geochim. Cosmochim. Acta 57 (1993) 1567–1586.

[23] L.P. Keller, K.L. Thomas, R.N. Clayton, T.K. Mayeda, J.M. DeHart, D.S. McKay, Aqueous alteration of the Bali CV3 chondrite: Evidence from mineralogy, mineral chemistry, and oxygen isotopic compositions, Geochim. Cosmochim. Acta 58 (1994) 5589–5598.

[24] M.E. Zolensky, K. Nakamura, M. Gounelle, T. Mikouchi, T. Kasama, O. Tachikawa, E. Tonui, Mineralogy of Tagish Lake: An ungrouped type 2 carbonaceous chondrite, Meteorit. Planet. Sci. 37 (2002) 737–761.

[25] J.F. Kerridge, J.D. Macdougall, K. Marti, Clues to the origin of sulfide minerals in CI chondrites, Earth Planet. Sci. Lett. 43 (1979) 359–367.

[26] R.E. Folinsbee, J.A.V. Douglas, J.A. Maxwell, Revelstoke, a new Type I carbonaceous chondrite, Geochim. Cosmochim. Acta 31 (1967) 1625–1635.

[27] A. Greshake, A. Bischoff, Chromium-bearing phases in Orgueil (CI): Discovery of magnesiochromite ($MgCr_2O_4$), ureyite ($NaCrSi_2O_6$), and chromiumoxide (Cr_2O_3), Lunar Planet. Sci. Conf. XXVII, 1996, pp. 461–462.

[28] C.E. Nehru, M.K. Weisberg, M. Prinz, Chromites in unequilibrated ordinary chondrites, Lunar Planet. Sci. Conf. XXVIII, 1997, pp. 9–10.

[29] M.N. Bass, Montmorillonite and serpentine in Orgueil meteorite, Geochim. Cosmochim. Acta 35 (1971) 139–147.

[30] T. Nakamura, K. Tomeoka, H. Takeda, Shock effects of the Leoville CV carbonaceous chondrite: A transmission

electron microscope study, Earth Planet. Sci. Lett. 114 (1992) 159–170.
[31] R. Okazaki, N. Takaoka, T. Nakamura, K. Nagao, Exposure history of the H chondrite Tsukuba, Proc. NIPR Symp. Antarct. Meteorites 23, 1998, pp. 117–119.
[32] M. Jungck, P. Eberhardt, Neon-E in Orgueil density separates, Meteoritics 14 (1979) 439–441.
[33] D.C. Black, On the origins of trapped helium, neon and argon isotopic variations in meteorites - II, Carbonaceous meteorites, Geochim. Cosmochim. Acta 36 (1972) 377–394.
[34] R.M. Walker, Nature of the fossil evidence: Moon and meteorites, in: R.O. Pepin, J.A. Eddy, R.B. Merrill (Eds.), Proc. Conf. Ancient Sun, Pergamon Press, New York, 1980, pp. 11–28.
[35] T. Nakamura, K. Nagao, N. Takaoka, Microdistribution of primordial noble gases in CM chondrites determined by in-situ laser microprobe analysis: Decipherment of nebular processes, Geochim. Cosmochim. Acta 63 (1999) 241–255.
[36] A.J. Brearley, Mineralogy of fine-grained matrix in the Ivuna CI carbonaceous chondrite, Lunar Planet. Sci. Conf. XXIII, 1992, pp. 153–154.
[37] H. Wänke, Der Sonnenwind als Quelle der Uredelgase in Steinmeteoriten, Z. Naturforsch. 20a (1965) 946–949.
[38] L.L. Wilkening, Particle track studies and the origin of gas-rich meteorites, Nininger Meteorite Award Paper, Arizona State University, Tempe, AZ, 1971.
[39] P. Pellas, Irradiation history of grain aggregates in ordinary chondrites, possible clues to the advanced stages of accretion, in: A. Elvius (Ed.), From Plasma to Planet, Wiley, New York, 1972, pp. 65–92.
[40] L. Schultz, P. Signer, J.C. Lorin, P. Pellas, Complex irradiation history of the Weston chondrite, Earth Planet. Sci. Lett. 15 (1972) 403–410.
[41] R.S. Rajan, On the irradiation history and origin of gas-rich meteorites, Geochim. Cosmochim. Acta 38 (1974) 777–788.
[42] E. Anders, Do stony meteorites come from comets?, Icarus 24 (1975) 363–371.
[43] K.R. Housen, L.L. Wilkening, C.R. Chapman, R. Greenberg, Asteroidal regoliths, Icarus 39 (1979) 317–351.
[44] K. Keil, Composition and origin of chondritic breccias, in: G.J. Taylor (Ed.), Workshop on Lunar Breccias and Soils and Their Meteoritic Analogs, Rep. 82-02, LPI Tech., Houston, TX, 1982, pp. 65–83.
[45] W. Nozaki, T. Nakamura, T. Noguchi, Experimental reproduction of micrometeorites by pulse-heating of carbonaceous chondrites, Proc. NIPR Symp. Antarct. Meteorites 27, 2002, pp. 132–133.
[46] K. Matsuoka, T. Nakamura, Y. Nakamuta, N. Takaoka, Yamato-86789: A heated CM-like carbonaceous chondrite, Antarct. Meteor. Res. 9 (1996) 20–36.
[47] A. Bischoff, A.E. Rubin, K. Keil, D. Stöffler, Lithification of gas-rich chondrite regolith breccias by grain boundary and localized shock melting, Earth Planet. Sci. Lett. 66 (1983) 1–10.
[48] J.A. Tyburczy, X. Xiaomei, J.A. Thomas, S. Epstein, Shock-induced devolatilization and isotopic fractionation of H and C from Murchison meteorite: some implications for planetary accretion, Earth Planet. Sci. Lett. 192 (2001) 23–30.
[49] H.Y. McSween, D.W.G. Sears, R.T. Dodd, Thermal metamorphism, in: J.F. Kerridge, M.S. Matthews (Eds.), Meteorites and the Early Solar System, University of Arizona Press, Tucson, AZ, 1988, pp. 102–113.
[50] T. Nakamura, K. Nagao, K. Metzler, N. Takaoka, Heterogeneous distribution of solar and cosmogenic noble gases in CM chondrites and implications for the formation of CM parent bodies, Geochim. Cosmochim. Acta 63 (1999) 257–273.
[51] O. Eugster, Cosmic-ray production rates for ^{3}He, ^{21}Ne, ^{38}Ar, ^{83}Kr, and ^{126}Xe in chondrites based on ^{81}Kr-Kr exposure ages, Geochim. Cosmochim. Acta 52 (1988) 1649–1662.
[52] S. Yoneda, M. Shima, K. Komura, K. Nagao, A. Okada, N.T. Kita, S. Togashi, Y. Okuyama, M. Bunno, A new meteorite shower, Tsukuba: Detection of ^{24}Na and the exposure history, Meteorit. Planet. Sci. 31 (1996) A157–A158.